Journal of Naval Sciences and Engineering
2022, Vol. 18, No. 2, pp. 251-279
Naval Architecture and Marine Engineering/Gemi İnşaatı ve Gemi Makineleri Mühendisliği

RESEARCH ARTICLE

**An ethical committee approval and/or legal/special permission has not been required within the scope of this study.*

INVESTIGATION OF THE EFFECT OF THE FLOW REGULATORS ON THE FLOW AROUND A GENERIC SUBMARINE SAIL*

Gökay SEVGİ[1, 2]
Barış BARLAS[3]
Uğur Oral ÜNAL[4]

[1]Istanbul Technical University, Department of Naval Architecture and Marine Engineering, Istanbul, Turkey,
sevgig@itu.edu.tr

[2]STM Inc., Naval Projects Directorate, Istanbul, Turkey,
gokay.sevgi@stm.com.tr

[3]Istanbul Technical University, Department of Naval Architecture and Marine Engineering, Istanbul, Turkey,
barlas@itu.edu.tr

[4]Istanbul Technical University, Department of Naval Architecture and Marine Engineering, Istanbul, Turkey,
ounal@itu.edu.tr

Received: 28.02.2022 **Accepted: 17.05.2022**

ABSTRACT

In this study, the viscous flow field around the mainsail of the DARPA Suboff AFF8 generic submarine fitted with two flow regulators in tandem configuration was investigated by means of computational fluid dynamics. An effective solution for the improvement of the mainsails of some of the current submarine classes of the Turkish Navy was aimed by covering the prepositioned periscopes by the flow regulators to avoid drag and vorticity increases due to the complex flow structure generated by these appendages and to provide a smoother flow topology. Three different NACA profiles with the same chord and span lengths were specified for regulating the flow. The effect of the NACA profile geometries on the hydrodynamic resistance and the flow field characteristics around the sail was demonstrated. It was shown that different profiles selected for the flow regulators considerably affect the computed resistance, velocity, pressure and vorticity characteristics of the flow field around the flow regulators. However, the flow structure at the side zones of the mainsail was not affected by the flow regulators. The profiles selected from NACA 6-digit and NACA 16-digit series give better hydrodynamic performance than their classical NACA 4-digit equivalent.

Keywords: *Submarine, Tandem Hydrofoils, Computational Fluid Dynamics, RANS.*

Investigation of the Effect of the Flow Regulators on the Flow Around a Generic Submarine Sail

AKIŞ DÜZENLEYİCİLERİN BİR JENERİK DENİZALTI YELKENİ ETRAFINDAKİ AKIŞA ETKİSİNİN İNCELENMESİ

ÖZ

Bu çalışmada, üzerine tandem konfigürasyonda iki akış düzenleyicinin konumlandırıldığı jenerik DARPA Suboff AFF8 denizaltısının yelkeni etrafında gelişen viskoz akım alanı hesaplamalı akışkanlar dinamiği ile incelenmiştir. Türk Donanması'nın mevcut denizaltı sınıflarından bazılarının ana yelkenlerinin iyileştirilmesi için periskopların oluşturduğu karmaşık akış yapısından kaynaklanan direnç ve girdaplılık artışlarını önlemek ve daha düzgün bir akış topolojisi sağlamak maksadıyla, önceden konumlandırılmış bu takıntılar akış düzenleyiciler ile çevrelenerek efektif bir çözüm hedeflenmiştir. Akışı düzenlemek için aynı kiriş ve açıklık boyuna sahip üç farklı NACA profili belirlenmiş ve bu NACA profili geometrilerinin hidrodinamik dirence ve yelken etrafındaki akım alanı karakteristiğine etkisi gösterilmiştir. Akış düzenleyiciler için seçilen farklı profillerin, akış düzenleyicilerin etrafındaki akım alanı için hesaplanan direnç, hız, basınç ve girdaplılık karakteristiklerini önemli ölçüde etkilediği görülürken ana yelkenin yan bölgelerindeki akım yapısını etkilemediği gözlemlenmiştir. NACA 6 ve NACA 16 serilerinden seçilen profiller, klasik NACA 4 serisi eşdeğerlerinden daha iyi bir hidrodinamik performans vermektedir.

Anahtar Kelimeler: *Denizaltı, Tandem Hidrofoiller, Hesaplamalı Akışkanlar Dinamiği, RANS.*

1. INTRODUCTION

The design of a submarine and its appendages with respect to hydrodynamics point of view is one of the most critical stages in overall submarine design since providing a minimized hydrodynamic resistance force exerted on it and a minimized acoustic signature are vital for its operability and secrecy. However, during the modernization activities carried out for a submarine, longer periscopes than the existing ones may need to be integrated into the submarine and this situation may result in the upper parts of the new periscopes to be outside of the submarine sail and thus may disrupt the hydrodynamic design of the submarine form. In such situations, it is required that these periscopes must be covered by some hydrofoil appendages which are also called flow regulators to avoid from the negative hydrodynamic effects of the periscopes being directly opened to the seawater. The forms of these flow regulators which are usually in tandem configuration must be optimized as an appendage design by taking into consideration of the restrictions such as the fixed positions of the periscope outlets and the hydrodynamic interaction between them.

Various researchers have investigated the flow around the submarines and their appendages to optimize their form by reducing their hydrodynamic resistance. In this context, Kale (2020) investigated the hydrodynamic resistance of a bare and an appended generic DARPA Suboff form by using a commercial code as well as an open-source code. Takahashi and Sahoo (2019) studied the resistance forces and moments exerted onto a DARPA Suboff submarine for straight translation and turning conditions. Lungu (2019) solved the flow problem around a DARPA Suboff form unsteadily by both detached eddy simulation and explicit algebraic stress model and analysed the computed wake behind the hull. Kukner et al. (2016) focused on the pressure distribution on a submarine for different forward speeds and examined the effect of the sail and the stern appendages on the computed hydrodynamic pressures on the hull. Budak and Beji (2016) executed a numerical investigation for nine different variants of a bare DARPA Suboff generic submarine model by keeping its body as the basis and varying the bow and stern sections in order to obtain an improved geometrical form. On the other hand, Chase (2012) executed a detailed investigation to compute

and visualize the hydrodynamic drag characteristics of a DARPA Suboff generic submarine model with appendages by using an in-house code. Wilson-Haffenden et al. (2010) conducted both numerical simulations and towing tank experiments for a bare DARPA Suboff submarine model which operates near the free surface in different submergence depths and Froude numbers to show the effect of the wave-making resistance on the total resistance. Baker (2004) also presented a methodology on how to model the boundary layer flow developed around a bare submarine form used for the studies of DRDC - Atlantic by means of computational fluid dynamics methods and validated his results with the experimental data from the wind tunnel tests.

The researches to investigate the hydrodynamic interaction between tandem hydrofoils with respect to varying distances, angles of attack and profiles have also been carried out by some researchers. Shang and Horrillo (2021) studied two two-dimensional NACA 0012 profiles aligned in tandem configuration for 788 combinations of different parameters such as spacing between the profiles and angles of attack of upstream and downstream profiles by a commercial code and artificial neural network method. Moreover, Maraam et al. (2021) examined two NACA 4412 profiles in two-dimension numerically in single-phase and multi-phase flows and showed the free surface effect on the results for varying submergence depths, distances between the profiles and angles of attack by using a commercial code. They also considered the cavitation occurrence on tandem profiles in their study. In the study of Chao et al. (2017), different combinations in sizes and kinematics of two hydrofoils in tandem configuration were investigated for the purpose of the reduction in drag forces. Furthermore, Kinaci (2015) approached to the problem of the hydrodynamic interaction between tandem hydrofoils in a different way. He used an iterative boundary element method and a Reynolds-averaged Navier-Stokes method to investigate the results for six different parameters in potential flow and viscous flow, respectively.

In the literature survey, although it was identified that several researches were conducted on the flow around submarines, their appendages and isolated tandem hydrofoils, there exist no study that deals with the

hydrodynamic interaction between tandem hydrofoils located on a submarine sail. In light of this, the present study focuses on merging these two subjects by considering a tandem hydrofoil system fitted on a generic submarine sail. This configuration is a widely encountered problem in engineering of the submarines, which aims to cover the prepositioned periscopes to avoid drag and vorticity increases due to the complex flow structure generated by these appendages and to provide a smoother flow topology.

In the context of the present study, the effect of the NACA profile geometry of the two flow regulators in the tandem configuration on the viscous flow around a generic submarine sail was investigated. The geometrical parameters such as the chord and span lengths of these flow regulators were kept constant in all cases investigated to solely evaluate the effect of the NACA profile geometry on the flow structure and hydrodynamic characteristics by means of computational methods. Accordingly, an effective solution for the improvement of the mainsails of some of the current submarine classes of the Turkish Navy was aimed.

2. GEOMETRIES

The submarine sail geometry used in the case studies was derived from the sail of the DARPA Suboff AFF8 submarine model which is a widely used geometry in the associated literature whose geometrical data is available in (Groves et al., 1989). The sail of this generic submarine model was scaled to give the sail length of 10.55 m, which approximately corresponds to the mainsail length of some of the submarine classes in the Turkish Navy. Hence the full-scale geometry of the sail was considered in the computations. The scaled mainsail used in the study has a height of 6.32 m and maximum breadth of 1.9 m. A view of the derived mainsail from the DARPA Suboff AFF8 submarine model is shown in Figure 1.

Figure 1. DARPA Suboff AFF8 submarine sail used in the case studies.

In this study, the following three cases were investigated.

- The case that the flow regulators on the submarine sail are NACA 66-021 profile shaped from NACA 6-digit series.
- The case that the flow regulators on the submarine sail are NACA 0021 profile shaped from NACA 4-digit series.
- The case that the flow regulators on the submarine sail are NACA 16-021 profile shaped from NACA 16-digit series.

From a hydrodynamic point of view, a slender form of the flow regulators is desirable to obtain lower resistance values, whilst the regulators should be thick enough to be able to cover the appendages of the sail such as the search and attack periscopes, etc. By taking these limitations into consideration, in all computational cases, the maximum thicknesses in percent of the chord lengths of the profiles from different NACA series were retained as 21%. All the profiles of the flow regulators were also

selected to be symmetrical with respect to their chord lines which means that these profiles have no camber. The representative section views of the selected profiles for the cases are shown in Figure 2.

The coordinates required to create the curves of the profiles were extracted from the data provided by Abbott and von Doenhoff (1959) in the stage of three-dimensional modelling of the geometries for the specified cases. In all the cases investigated, the chord and the span lengths of these flow regulators were kept constant while their positions are fixed on the submarine sail. The prepared three-dimensional geometries for the cases are shown in Figure 3.

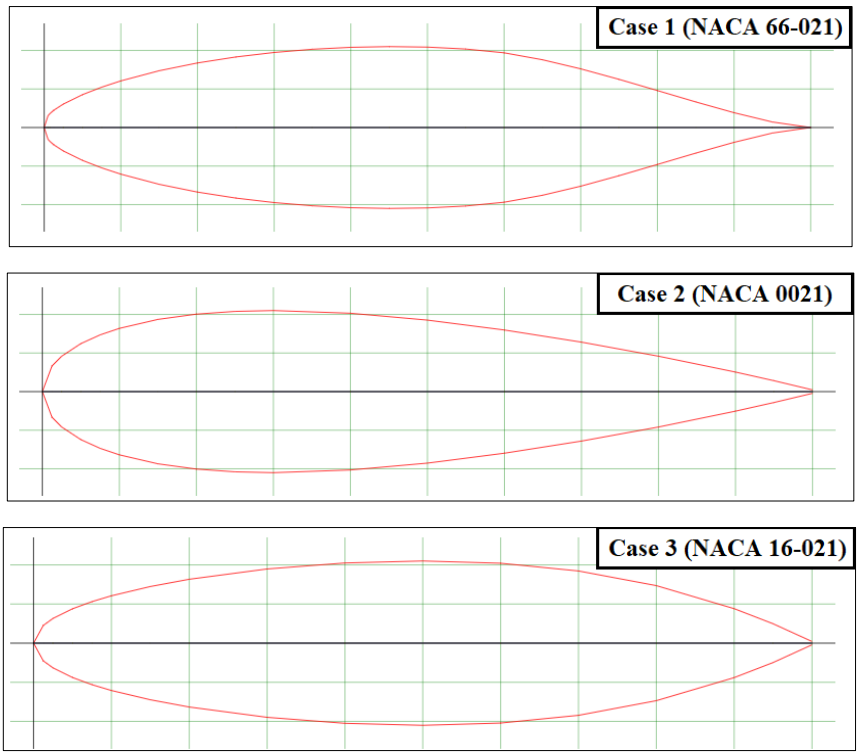

Figure 2. Representative section views of the selected profiles for the cases.

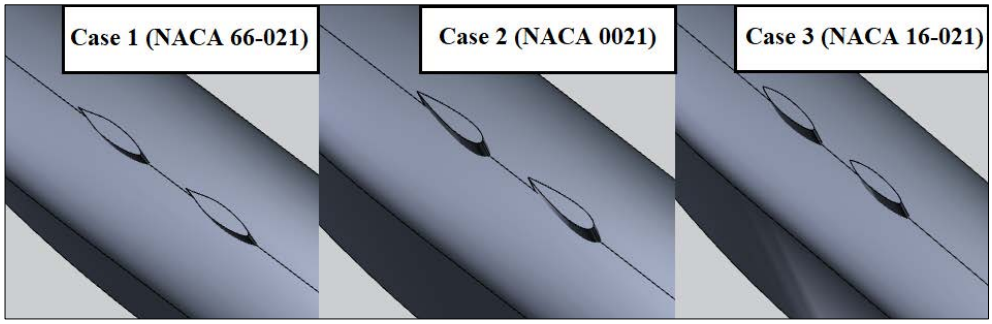

Figure 3. Prepared geometries for the cases.

3. COMPUTATIONAL DETAILS

3.1. Governing Equations and Numerical Technique

Incompressible steady Reynolds-averaged Navier-Stokes (RANS) equations (Wilcox, 2006) were solved by means of finite volume discretisation to compute the viscous flow around the mainsail and flow regulators. An unsteady approach will perhaps increase the accuracy; however, it will also significantly affect the computational time and resource demand. Since the work presented is mainly a comparative study, the steady approach would provide reliable hydrodynamic assessments. In Cartesian tensor notation, the above equations can be expressed as follows:

$$\frac{\partial U_i}{\partial x_i} = 0 \tag{1}$$

$$\rho \frac{\partial U_j U_i}{\partial x_j} = -\frac{\partial P}{\partial x_i} + \frac{\partial}{\partial x_j}(\mu S_{ij} - \overline{\rho U_i' U_j'}) \tag{2}$$

In these equations; ρ, μ, P, U and U' denote fluid density, dynamic viscosity, average static pressure, average velocity and fluctuating velocity, respectively. S_{ij} represents the average strain rate tensor and the term $\overline{\rho U_i' U_j'}$ indicates the Reynolds stresses which imply the turbulent fluctuations. The line over this term means the term is averaged. In order to solve the turbulence field, Shear Stress Transport k-ω turbulence model of Menter (1994) which computes the Reynolds stress tensor by Boussinessq

hypothesis (Tennekes and Lumley, 1972) was employed. Pseudo transient computation was utilized in all the computational analyses and the hybrid initialization technique was used before starting the computations. The details for pseudo transient computation and the hybrid initialization technique are available in the documentation by ANSYS Inc. (2013).

The pressure and velocity coupling problem was solved by standard coupled scheme which solves the aforementioned momentum and pressure-based continuity equations simultaneously and distance-based Rhie-Chow interpolation method was chosen for the flux type (Rhie and Chow, 1983). Furthermore, second order approach was employed for the spatial discretization of the convective variables while the gradient was discretized by least squares cell-based method. The theory of these numerical methods can be found in Pletcher et al. (2011). On the other hand, the iterations were run until the scaled residuals of continuity, momentum and turbulence equations decreased to 10^{-4} in all computations. The convergences of the resistance forces of the front flow regulators, the back flow regulators and the total resistances were also monitored according to the number of iterations in all the cases.

3.2. Computational Domain, Boundary Conditions and Mesh Structure

The computational domain was created to be a rectangular prism-shaped domain. Since the computations involve slender bodies, extremely large domain dimensions were not considered. The inflow and outflow boundaries were placed at L and 2L, respectively, from the submarine sail, where L denotes the length of the submarine sail. The sail was also located in the centreline of the specified 2L width in the base plane of the computational domain. Moreover, the computational domain was given a height of 1.5L starting from the baseline of the submarine sail. The additional simulations performed with larger domain sizes led to no appreciable changes in the results. A smaller rectangular prism was also created in order to generate more refined grids in the wake region of the flow regulators. A general view of the computational domain can be seen in Figure 4.

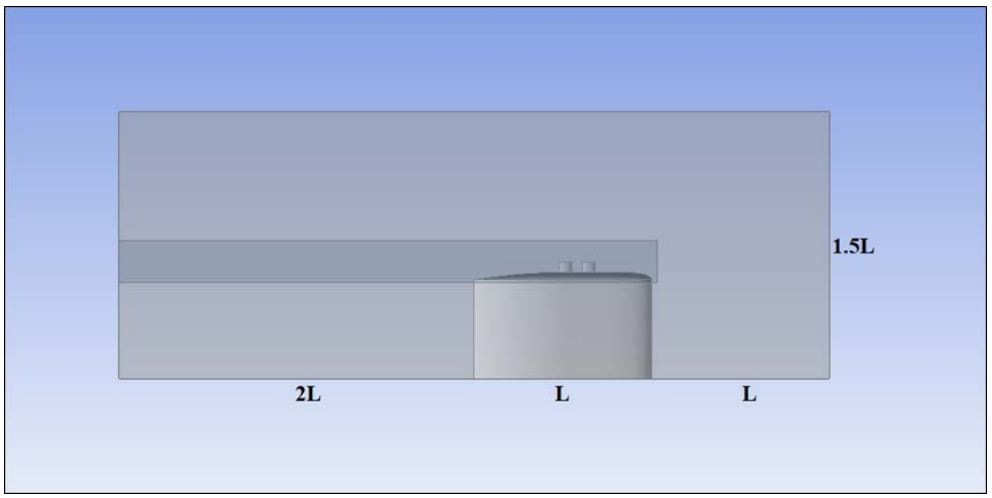

Figure 4. Profile view of the computational domain.

Liquid water was defined as the working fluid of the computational domain and 1025 kg/m^3 of density was assumed for liquid water. The entrance of the fluid to the computational domain was defined as velocity-inlet whose velocity is 20 knots in magnitude as normal to boundary which corresponds to a Reynolds number of approximately 10^7 for the mainsail geometry. It is of note that the flow velocity selected also corresponds to the submerged maximum speed of some of the submarine classes of the Turkish Navy. Furthermore, the exit of the fluid from the computational domain was defined as pressure-outlet where 0 Pa gauge pressure was assigned. For both velocity-inlet and pressure-outlet boundary conditions, turbulent intensity and turbulent viscosity ratio were defined as 5% and 10, respectively. On the other hand, the lateral surfaces of the computational domain were selected as symmetry boundary condition. Moreover, the geometric components such as the mainsail and the flow regulators were defined as wall boundary condition to solve the near wall regions by wall function to avoid the long solution times of viscous layer. Also, no slip condition and smooth surface condition were assumed at walls. The depiction of the specified boundary conditions can be seen in Figure 5.

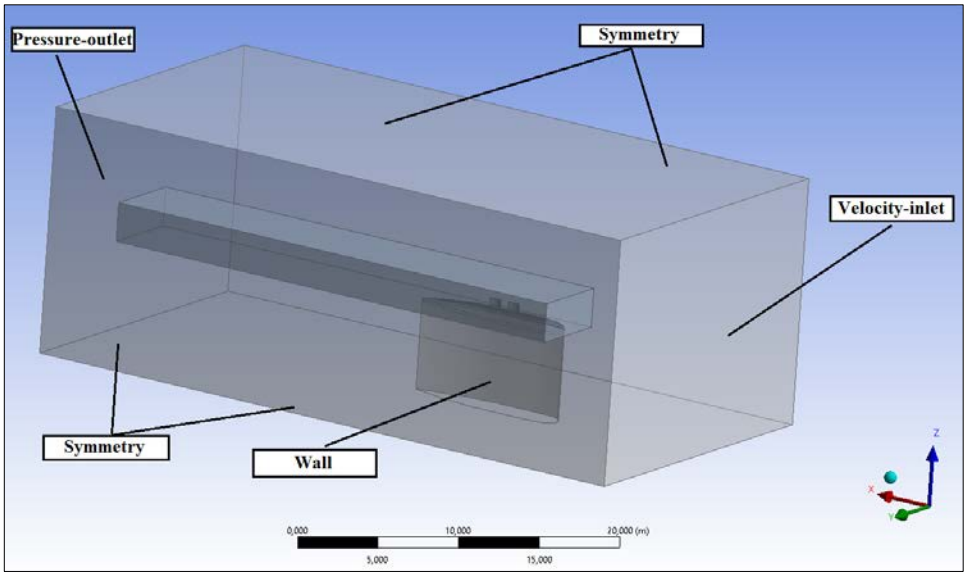

Figure 5. Boundary conditions.

An unstructured grid system with tetrahedral elements was used to discretize the computational domain for all the cases. In order to better model the boundary layer on the near wall regions of the sail and the flow regulators, the sizes of the elements were systemically kept low in these regions. In order to achieve this, advanced face sizing functions of the mesh generation software used with high smoothing and slow transition were employed. It was also benefited from the local mesh controls options for further improvement of the quality of the mesh structure. Since the Reynolds number considered is rather high, the boundary layer could not be fully resolved up to the viscous sublayer. The non-dimensional distance from the walls of the mainsail and the flow regulators was kept around y^+=50. However, the enhanced wall functions approach of the flow solver was employed which uses a blending function for a single wall law for the entire wall region. This approach made the use of the turbulence model selected possible. Also, the numbers of the elements were intentionally increased in the wake region of the flow regulators in order to predict the vorticities and velocities due to the flow regulators more accurately. Moreover, the same resolution parameters were employed for all the cases and thus similar grid sizes were obtained for all considered cases. However,

the final grid resolution to be used in computational analyses was specified after the verification study to be explained in detail in Section 4.

4. VERIFICATION STUDY

In order to make sure whether the computational results were independent from the grid resolution, a verification study was carried out. Grid Convergence Index (GCI) calculation which was introduced by Celik et al. (2008) was executed to verify the results. For the verification study, Case 1 was selected and three grids in different resolutions were generated for this case by considering that the grid spacing ratio between the successive two grids to be greater than 1.3 as recommended by Celik et al. (2008). In the end of the verification study, the grids of element numbers of approximately 1.04 M, 2.38 M and 5.51 M were generated for the coarse, medium and fine grids, respectively. The grid dependency results for the total resistance for Case 1 are given in Table 1. In the table, e and GCI represent the relative error between the results and the numerical discretization uncertainty for the total resistance value in percent, respectively.

Table 1. Grid dependency for the total resistance values of Case 1.

Grid Resolution	Total Resistance (kN)	e (%)	GCI (%)
Coarse	34.0	-	-
Medium	33.2	2.4	3.6
Fine	32.7	1.5	2.0

A monotonic convergence can be identified from the numerical results presented in the table. The relative errors and the discretization uncertainties gradually decrease when the grid resolution is increased. The final GCI value of the fine grid structure was calculated as 2% for the total resistance value. Further refinement of the discretization of the computational domain was, hence, not needed and the structure of the fine grid was decided to be used for the other cases. The general view of the fine grid structure is depicted in Figure 6.

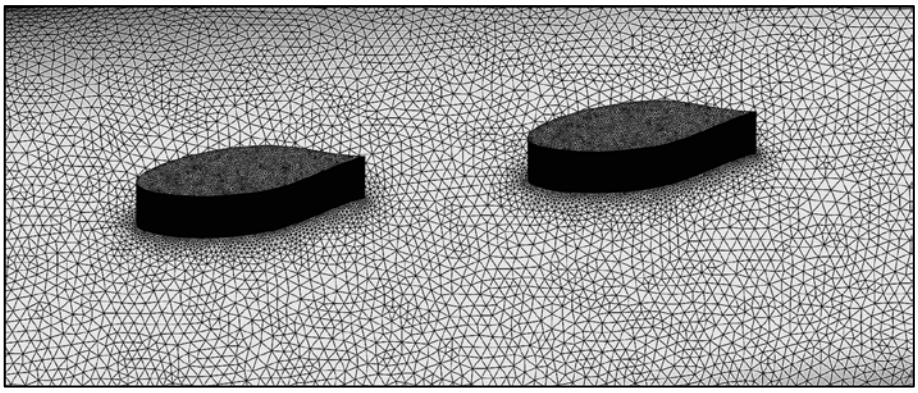

Figure 6. The general view of the fine grid structure.

5. RESULTS AND DISCUSSION

5.1. Resistance Computations

The obtained resistance values from the computational analyses by using the verified fine grid structure for the three cases explained previously are shown in Table 2. In this table, the approximate element numbers created when this verified fine grid structure is employed for these cases are also presented.

Table 2. General computation results obtained from the investigated cases.

Case	Element Number ($x10^6$)	Total Resistance (kN)	Resistance of Front Flow Regulator (N)	Resistance of Back Flow Regulator (N)
Case 1	5.51	32.7	285.5	594.0
Case 2	5.49	32.9	331.9	643.2
Case 3	5.50	32.8	293.0	654.1

The numerical data obtained from the computational analyses show that Case 1 with a flow regulator profile NACA 66-021 gives the best resistance results. It can also be seen from Table 2 that Case 2, where NACA 0021 profile was selected for the flow regulators, gives the highest resistance.

However, it was seen that there are not so many differences between the results with respect to the total resistance values. Moreover, the resistance of back flow regulator was computed 94% to 123% higher than the resistance of front flow regulator in all the cases. It is assessed that this situation occurs due to the impact of the vortices formed while the fluid is passing through the front flow regulator.

5.2. Flow Fields

The contours of the velocity magnitudes around the mainsail at the plane z = 2.4 m, which is 2.4 m above the centre of gravity of the sail is depicted in Figure 7. The flow direction is from left to right. The location of the plane is very close to the top surface of the mainsail. It can be seen that the flow is nearly identical for all cases considered. This indicates that a large portion of the flow around the mainsail is essentially unaffected from the flow field generated by the flow regulators.

Shown in Figure 8 are the velocity magnitude distributions around the flow regulators at z=3.25 m, which is a plane slightly above the top surface of the mainsail. For all cases the fluid velocity is higher around the front flow regulator as expected. Due to its thicker leading-edge, highest velocity levels of above 13 m/s may be observed around the NACA 0021 profile. While higher flow speeds occur towards the second portion of the profiles for Case 1 and 3, Case 2 exhibits large velocities near the leading-edge. The interaction zone between the two regulators can be clearly seen in all cases. The lowest velocity levels are displayed by Case 3.

The velocity magnitude distributions at z=3.7 m, which corresponds to a horizontal level close to the top surface of the regulators, can be seen in Figure 9. It may be observed that the levels are much lower than those encountered at the plane close to the mainsail due to the effect of the tip vortices arising from the open end of the regulators. Large differences detected between the flow structures around the front and back flow regulators are also due to the helical motion created by the tip vortices. The zones that are strongly affected by the helical motion are apparent towards to trailing edge of the profiles for Case 1 and 3. For Case 2, the beginning of same zone is close to the midsection of the regulator. The velocity

distributions around the back flow regulator of Case 2 and 3 exhibit significantly lower levels than those of Case 1.

The non-dimensional pressure distributions on the surfaces of the flow regulators and the mainsail can be examined in Figure 10. Due to its thicker leading edge form, the pressure levels at the leading edge region of Case 2 are higher than those of the leading edge regions of Case 1 and Case 3. For the same reason, the suction zone following the leading edge is larger and the level of the suction is stronger in Case 2. A smoother pressure distribution can be observed in Case 3. The pressure recovery of Case 1 appears to be rather high compared to the other two cases which can be identified by examining the high pressure zone around the trailing edge. Figure 11 presents the non-dimensional pressure contours at z=3.7 m. It can be seen that the effect of the adverse pressure gradient is more pronounced in Case 1 and 3. The weaker pressure recovery of the back flow regulators and the effect of the tip vortices on the pressure field in the wake of the front regulators are more clearly seen in the figure.

The iso surfaces of Q criterion may be examined in Figure 12. $Q=50\ s^{-2}$ were selected for a clearer presentation. The iso surfaces were coloured by the turbulent kinetic energy. For all cases, the organized vortex structures can be identified around the edges of the top surfaces of the flow regulators. For Case 2 and 3 the coherent structures around the front flow regulators nearly reach to the back flow regulator displaying an elongated form. Case 3 also presents large vortex structures on top of the mainsail in the zone between the two regulators and around the bottom edge of the back flow regulator. The turbulent intensity appears to be higher in Case 2 particularly around the top edges of the regulators whilst the other two cases exhibit a similar turbulence character. The plots indicate that Case 1 displays a better performance in terms of the vorticity characteristics.

The vorticity characteristics of the flow regulators are also presented in Figure 13 where the streamwise vorticity levels at the planes following the trailing edges of the regulators as well as the plane immediately before the leading edge of the back flow regulator. The traces of the two pairs of counter-rotating vortex structures are primarily apparent close the tip of the

regulators for all cases. Eventually the vortices emerging from the front flow regulator merges and a pair of counter-rotating vortices arrive to the back flow regulator. Smaller vortices are also notable along the trailing edges of the regulators for Case 2 and 3. The plots point out that the streamwise vorticity levels and the area of the affected zone are smaller in Case 1.

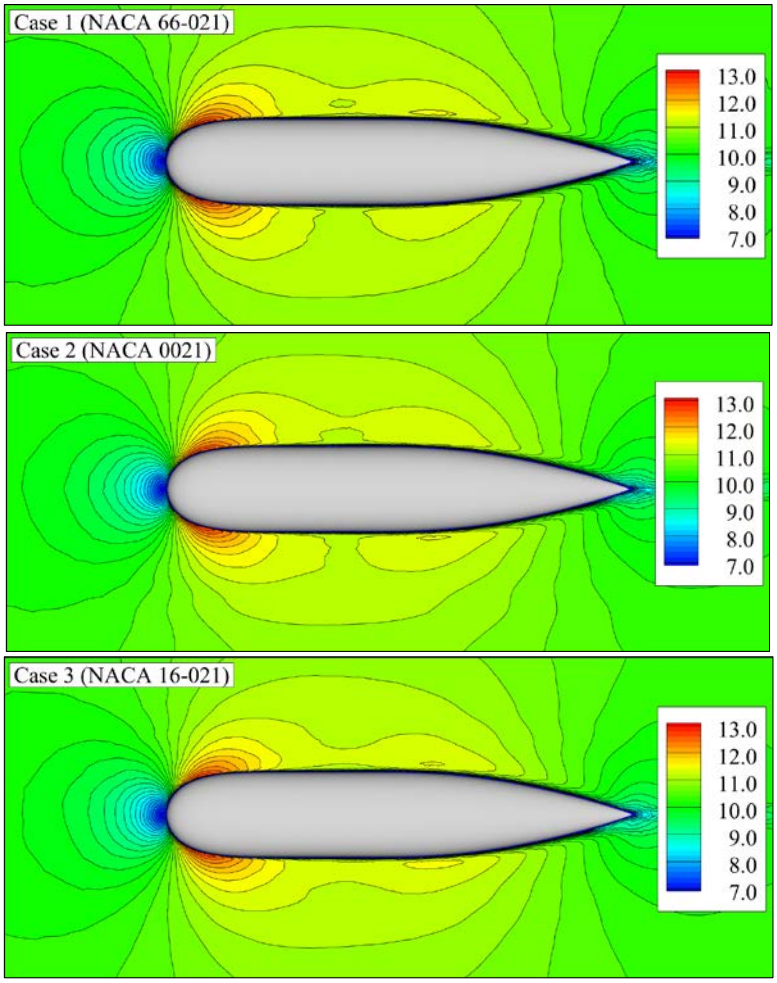

Figure 7. Contours of velocity magnitudes (m/s) around the mainsail at z = 2.4 m.

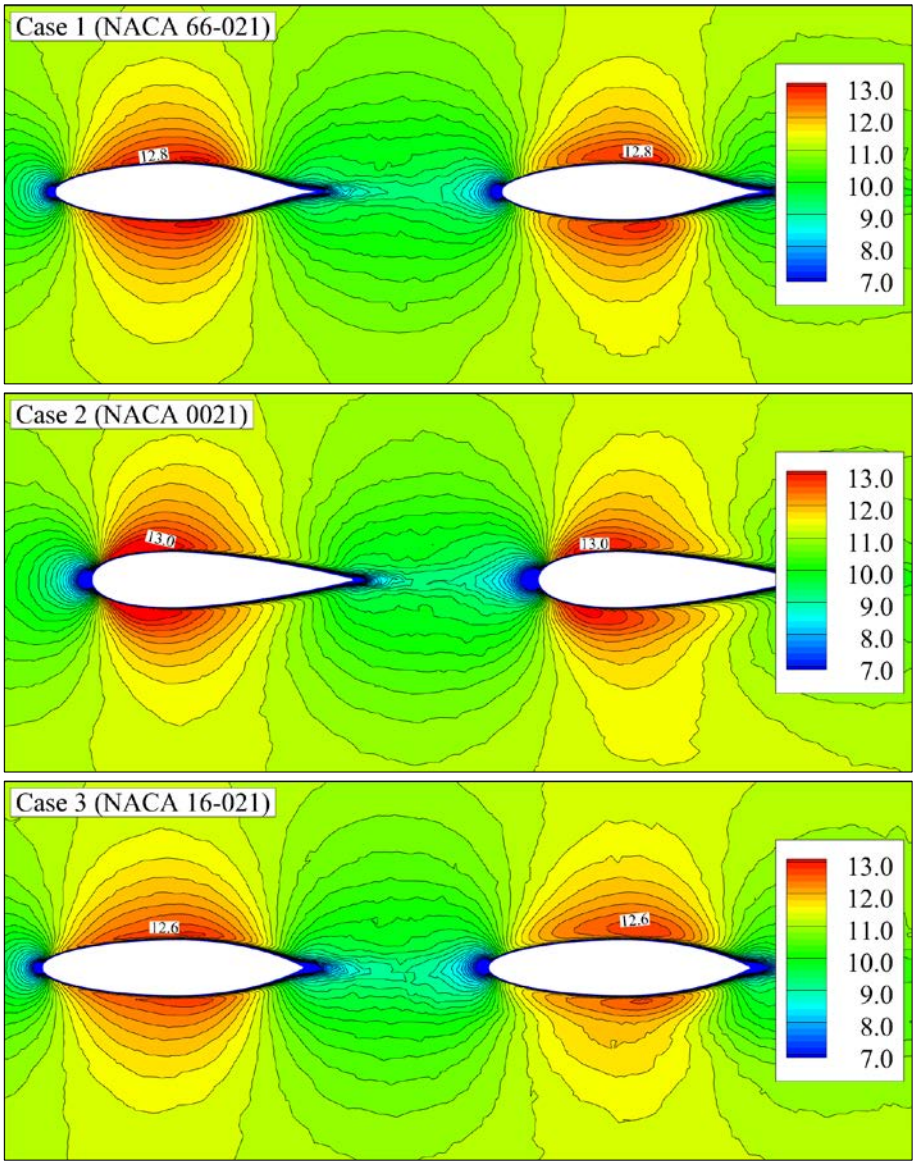

Figure 8. Contours of velocity magnitudes (m/s) around the flow regulators at z = 3.25 m.

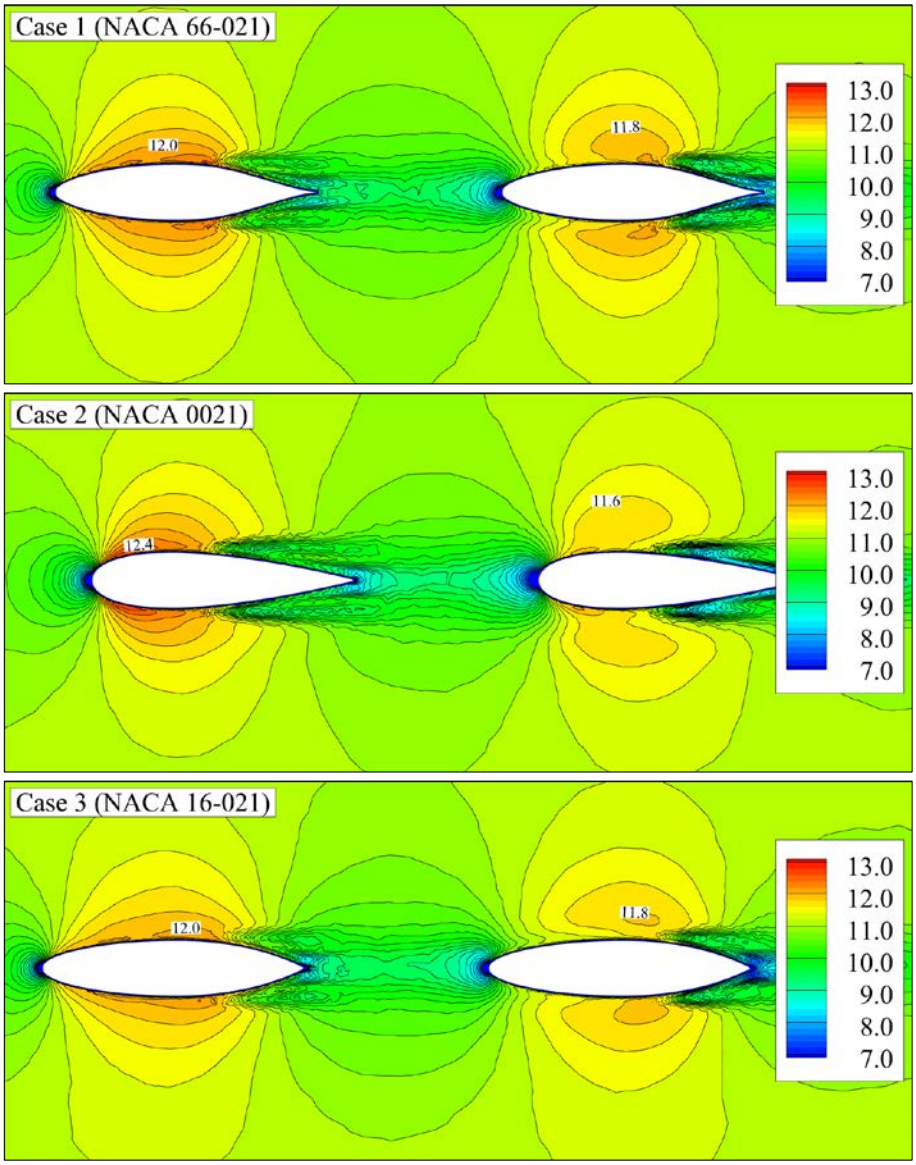

Figure 9. Contours of velocity magnitudes (m/s) around the flow regulators at z = 3.7 m.

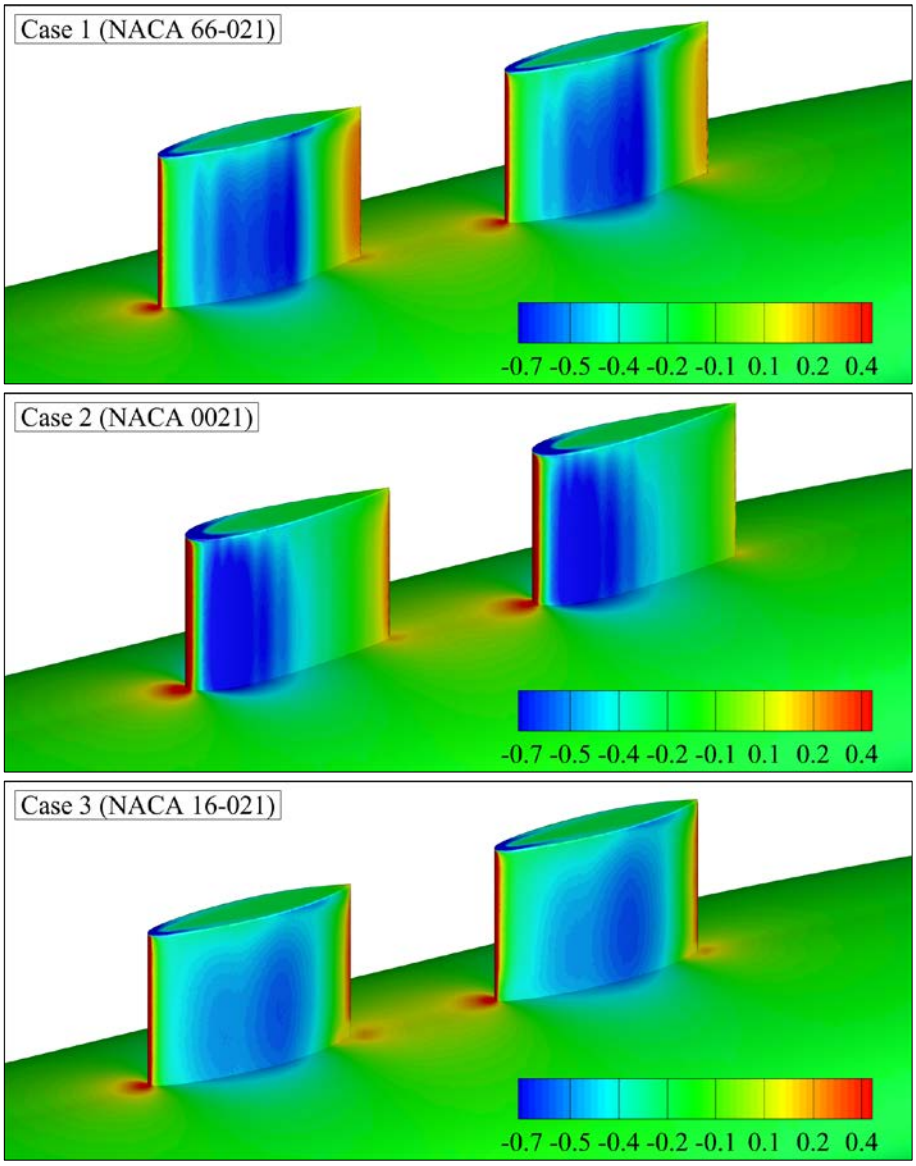

Figure 10. Non-dimensional pressure distributions on the surfaces of the flow regulators and the mainsail.

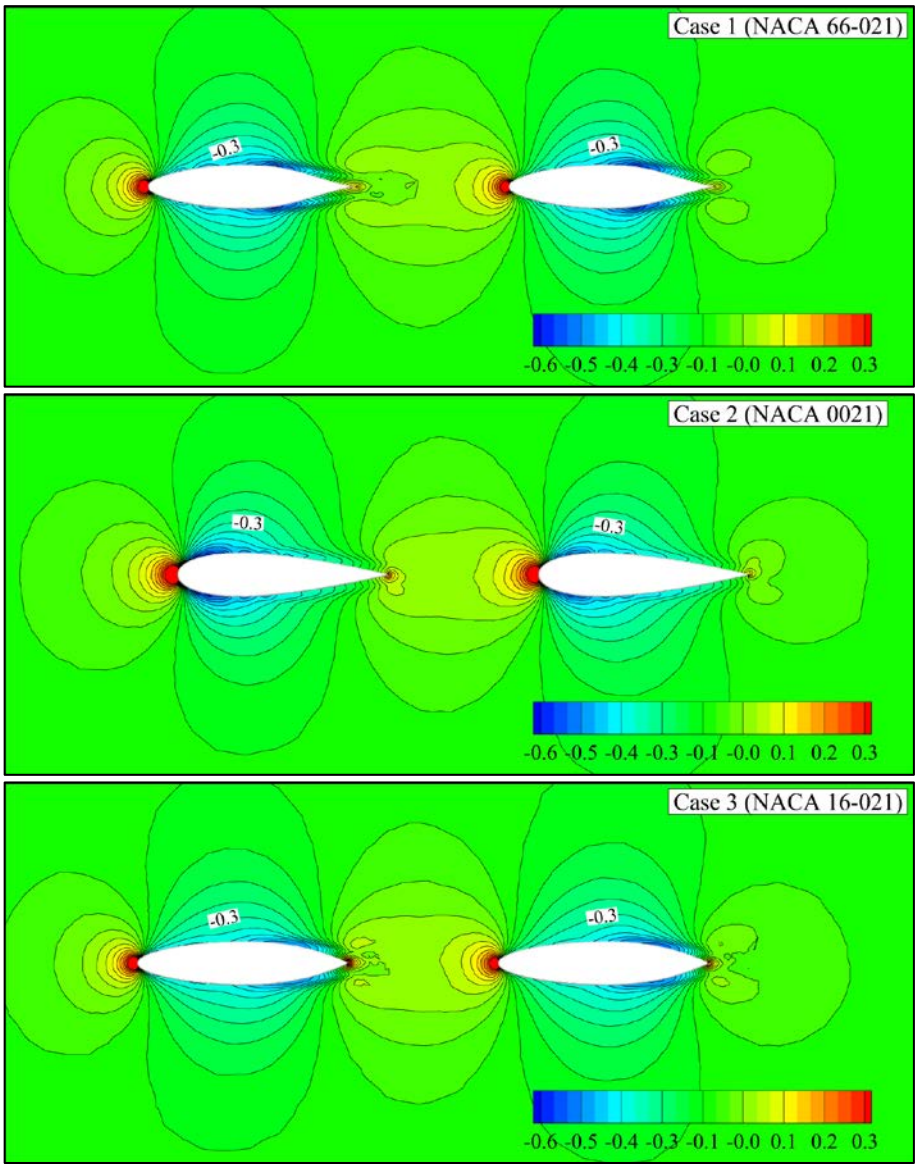

Figure 11. Non-dimensional pressure distributions around the flow regulators at z = 3.7 m.

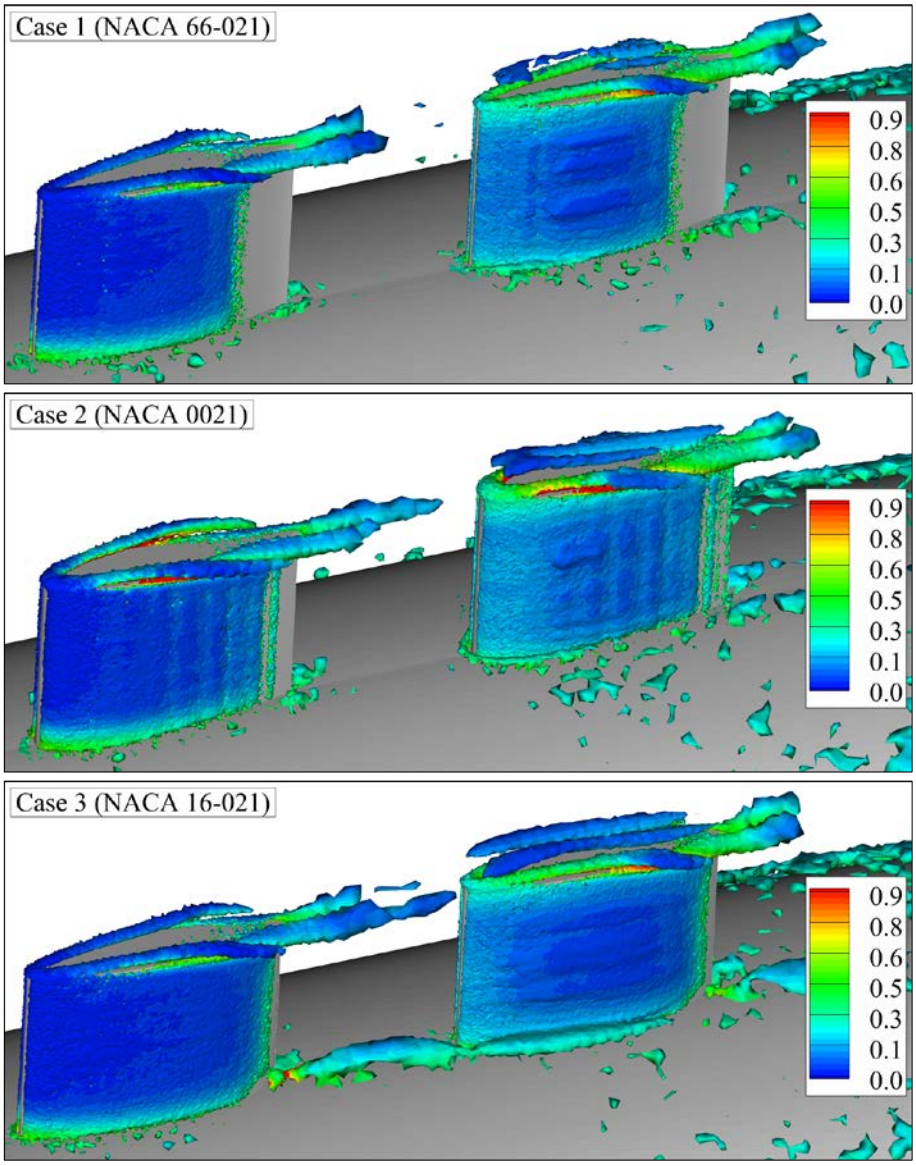

Figure 12. Q criterion iso surfaces around the flow regulators (Q=50 s^{-2}, coloured by turbulent kinetic energy, m^2s^{-2}).

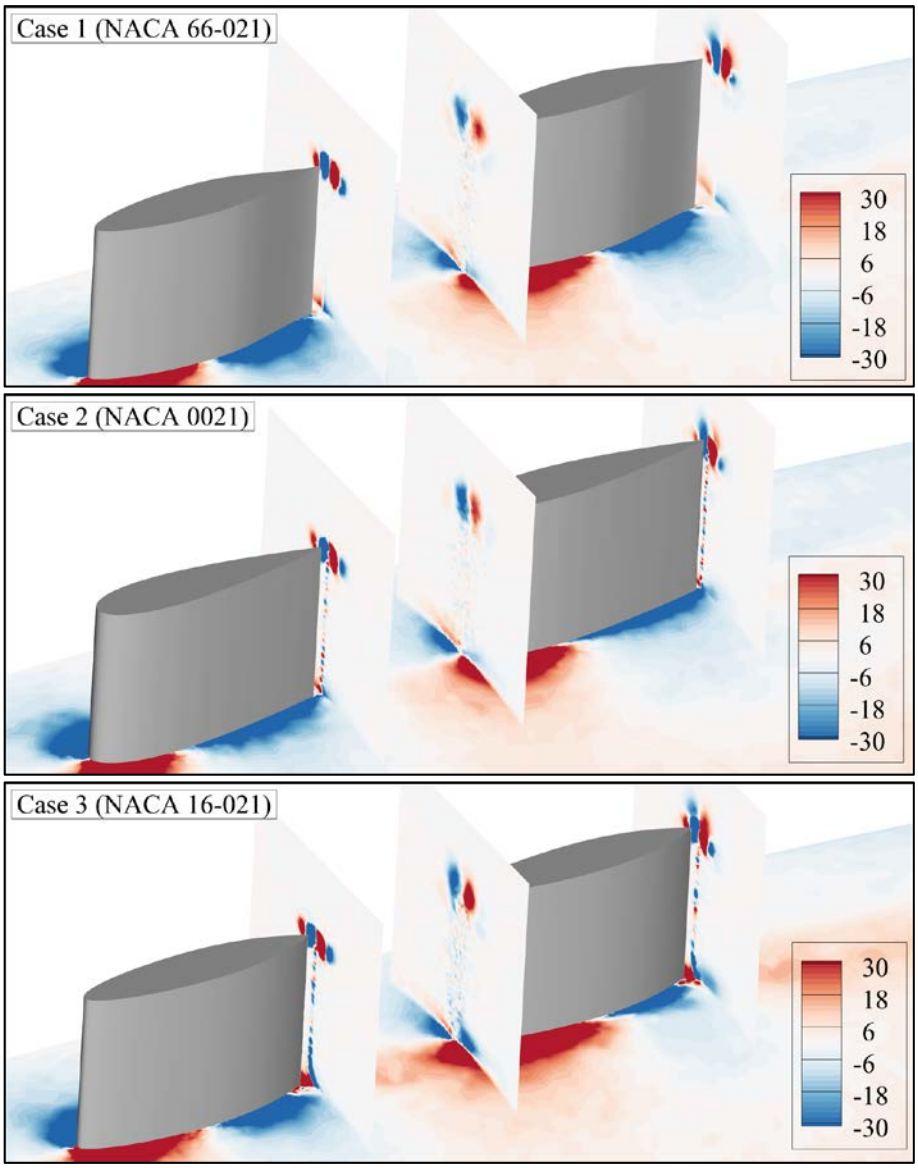

Figure 13. Streamwise vorticity levels (s^{-1}) at the vertical planes near the leading and trailing edges of the flow regulators.

6. CONCLUSION

In this study, the flow around a generic submarine sail with two flow regulators in tandem configuration assembled on it was investigated for three different cases. A scaled geometry derived from the mainsail of the DARPA Suboff AFF8 generic submarine model was used as the main platform. NACA 66-021, NACA 0021 and NACA 16-021 sectioned flow regulators with the same chord and span lengths at the fixed positions on the submarine sail were selected for the computational study in order to demonstrate the effect of the different profiles of the flow regulators on the flow characteristics. RANS computations were conducted by using the SST k-ω turbulence model at a Reynolds number of approximately 10^7.

It was shown that different profiles selected for the flow regulators considerably affect the computed resistance, velocity, pressure and vorticity characteristics of the flow field around the flow regulators. However, it was clearly identified that the flow structure at the sides of the mainsail was not affected by the flow regulators fitted as expected. Hence, most of the attention was paid to the region where the flow regulators exist. One of the most important outcomes was that a NACA 6-digit and a NACA 16-digit profile give better hydrodynamic performance than their classical NACA 4-digit equivalent in the same exact flow conditions for the flow around this submarine sail with respect to the total resistance values. Moreover, it was observed that Case 1 which gave the least computed resistance values in the study also displayed the least vorticity levels indicating that flow regulators with NACA 66-021 profile will also have an advantageous hydro-acoustic characteristic. It was also seen that the condition of the back flow regulator is highly critical as it is exposed to the vortices by the front flow regulator.

It is assessed that this study may be extended to include the hydro-acoustic analyses of noise generated by these flow regulators to examine the silent operability of this submarine sail. Moreover, a single larger flow regulator geometry that covers both periscope outlets can also be designed and analysed in the same flow conditions considered and its numerical results can be compared with the three cases investigated in the present study. The computational analyses for speeds slower than 20 knots can also be

conducted to more reliably obtain generalised results. Additionally, the cases discussed in this study may be analysed by a time-dependent RANS simulation which may provide more reliable results.

It is believed that this research article provides practical and encouraging information about the improvement of the hydrodynamic/hydro-acoustic characteristics of the current submarine classes of the Turkish Navy.

ACKNOWLEDGEMENT

The authors would like to thank STM Inc. for the valuable discussions related to the topic.

CONFLICT OF INTEREST STATEMENT

All authors declare that they have no conflicts of interest and no financial support was received for this study.

REFERENCES

Abbott, I. H., and von Doenhoff, A. E. (1959). *Theory of Wing Sections: Including a Summary of Airfoil Data*, Dover Publications Inc., New York, USA.

ANSYS Inc. (2013). *ANSYS Fluent User's Guide*, Canonsburg, USA.

Baker, C. (2004). "Estimating Drag Forces on Submarine Hulls". *Contract Report*, Defence Research and Development Canada - Atlantic, Canada.

Budak, B., and Beji, S. (2016). "Computational Resistance Analyses of a Generic Submarine Hull Form and Its Geometric Variants". *Journal of Ocean Technology*, Vol. 11, No. 2, 76-86.

Celik, I. B., Ghia, U., Roache, P. J., Freitas, C. J., Coleman, H., and Raad, P. E. (2008). "Procedure for Estimation and Reporting of Uncertainty due to Discretization in CFD Applications". *Journal of Fluids Engineering*, Vol. 130, Issue 7. doi:10.1115/1.2960953.

Chao, L. M., Zhang, D., and Pan, G. (2017). "Roles of Size and Kinematics in Drag Reduction for Two Tandem Flexible Foils". *Modern Physics Letters B*, Vol. 31, No. 33. doi:10.1142/S0217984917503110.

Chase, N. (2012). *Simulations of DARPA Suboff Submarine Including Self-propulsion with the E1619 Propeller*. [Master's Thesis]. The University of Iowa Graduate College, Iowa, USA.

Groves, N. C., Huang, T. T., and Chang, M. S. (1989). "Geometric Characteristics of DARPA Suboff Models". David Taylor Research Center, Bethesda, USA.

Kale, F. M. (2020). *Numerical Investigation of Flow around a Submarine by Openfoam and ANSYS Fluent*. [Master's Thesis]. Istanbul Technical University Institute of Science, Istanbul, Turkey.

Kinaci, O. K. (2015). "A Numerical Parametric Study on Hydrofoil Interaction in Tandem". *International Journal of Naval Architecture and Ocean Engineering*, Vol. 7, Issue 1, 25-40. doi:10.1515/ijnaoe-2015-0003.

Kukner, A., Duran, A., and Cinar, T. (2016). "Investigation of Flow Distribution around a Submarine". *Journal of Naval Science and Engineering*, Vol. 12, Issue 2, 1-26.

Lungu, A. (2019). "DES-based Computation of the Flow around the DARPA Suboff". *IOP Conference Series: Materials Science and Engineering*, 591. doi:10.1088/1757-899X/591/1/012053.

Maraam, M. A., Ghafari, H. R., Ghassemi, H., and Ghiasi, M. (2021). "Numerical Study on the Tandem Submerged Hydrofoils Using RANS Solver." *Mathematical Problems in Engineering*, Vol. 2021. doi:10.1155/2021/8364980.

Menter, F. R. (1994). "Two-equation Eddy-viscosity Turbulence Models for Engineering Applications". *AIAA Journal*, Vol. 32, No. 8, 1598-1605. doi:10.2514/3.12149.

Pletcher, R. H., Tannehill, J. C., and Anderson, D. A. (2011). *Computational Fluid Mechanics and Heat Transfer*, 3rd Edition. CRC Press, Florida, USA.

Rhie, C. M., and Chow, W. L. (1983). "Numerical Study of the Turbulent Flow Past an Airfoil with Trailing Edge Seperation". *AIAA Journal*, Vol. 21, No. 11, 1525-1532. doi:10.2514/3.8284.

Shang, Y., and Horrillo, J. J. (2021). "Numerical Simulation and Hydrodynamic Performance Predicting of 2 Two-dimensional Hydrofoils in Tandem Configuration". *Journal of Marine Science and Engineering*, Vol. 9, Issue 5, 462-477. doi:10.3390/jmse9050462.

Takahashi, K., and Sahoo, P. K. (2019). "Fundamental CFD Study on the Hydrodynamic Performance of the DARPA Suboff Submarine". *Proceedings of the 38th International Conference on Ocean, Offshore & Arctic Engineering*, Volume 2: CFD and FSI, Glasgow, UK.
doi: 10.1115/OMAE2019-96190.

Tennekes, H., and Lumley, J. L. (1972). *A First Course in Turbulence*, MIT Press, Cambridge, UK.

Wilcox, D. C. (2006). *Turbulence Modeling for CFD*, 3rd Edition, DCW Industries, California, USA.

Wilson-Haffenden, S., Renilson, M., Ranmuthugala, D., and Dawson, E. (2010). "An Investigation into the Wave Making Resistance of a Submarine Travelling below the Free Surface". *International Maritime Conference 2010: Maritime Industry - Challenges, Opportunities and Imperatives*, Sydney, Australia.